Simulation of the Impact of Fracturing-Fluid-Induced Formation Damage in Shale Gas Reservoirs

N. Farah and **D. Y. Ding,** IFP Energies Nouvelles; and **Y. S. Wu,** Colorado School of Mines

Summary

The unconventional gas resources from tight and shale gas reservoirs have received great attention in the past decade and have become the focus of the petroleum industry. Shale gas reservoirs have specific characteristics, such as tight reservoir rock with nanodarcy permeability. Multistage hydraulic fracturing is required for such low-permeability reservoirs to create very complex fracture networks and therefore to connect effectively a huge reservoir volume to the wellbore. During hydraulic fracturing, an enormous amount of water is injected into the formation, where only 25–60% is reproduced during flowback and a long production period. A major concern with hydraulic fracturing is the water-blocking effect in tight formations caused by the high capillary pressure and the presence of water-sensitive clays. High water saturation in the invaded zone near the fracture face may reduce gas relative permeability greatly and may impede gas production.

In this paper, we consider the numerical techniques to simulate during hydraulic fracturing the water invasion or formation damage and its impact on the gas production in shale gas reservoirs. Two-phase-flow simulations are considered in a large stimulated reservoir volume (SRV) containing extremely low-permeability tight matrix and multiscale fracture networks including primary hydraulic fractures, induced secondary fractures, and natural fractures.

To simulate the water-blocking phenomenon, it is usually required to explicitly discretize the fracture network and use very fine meshes around the fractures. On the one hand, the commonly used single-porosity model is not suitable for this kind of problem, because a large number of gridblocks is required to simulate the fracture network and fracture–matrix interaction. On the other hand, a dual-porosity (DP) model may also be not applicable, because of the long transient duration with large block sizes of ultralow-permeability matrix. In this paper, we study the applicability of the MINC (multiple interacting continuum) method, and use a hybrid approach between matrix and fractures to correctly simulate the fracturing-fluid invasion and its backflow during hydraulic fracturing. This approach allows us to quantify the fracturing water invasion and its formation-damage effect in the whole SRV.

Introduction

Most shale gas reservoirs are naturally fractured because they have low matrix permeability. In addition, the matrix contains the most gas volume, where global flow in the reservoir occurs through the network of primary hydraulic fractures, induced fractures, and stimulated natural fractures. Note that fractures play an important role in gas production from shale formations. Horizontal drilling and multistage hydraulic fractures are required and widely used to create a complex fracture network in a shale gas reservoir. An enormous amount of water is injected into the formation during the hydraulic-fracturing operation to create a large SRV, where only a fraction of pumped water (25–60%) can be reproduced during a long production period and the large remaining quantities of fracturing fluids are still blocked in the formation.

A major concern with hydraulic fracturing is the water-blocking effect in tight formation caused by high capillary pressure and the presence of water-sensitive clays. In addition, several mechanisms such as imbibition, relative permeability, gravity segregation, and stress-sensitive fracture conductivities will control the behavior of blocked water. High water saturation in the invaded zone near the fracture face will greatly reduce gas permeability and impede gas production.

Fracturing-fluid-induced formation damage has been studied in the literature for a long time (e.g., Holditch 1979; Friedel 2004; Gdanski et al. 2006; Wang et al. 2009; Ding et al. 2013). Recently, the fracturing-fluid-induced formation damage is particularly discussed for extremely low-permeability shale gas reservoirs. Li et al. (2012) used an analytical model to study fracture-face matrix damage in shale gas reservoirs. Cheng (2012) investigated the formation-damage effect with a numerical model. Agrawal and Sharma (2013) used a 3D numerical simulator to study the gravity effect. Bertoncello et al. (2014) compared experimental data and studied fracturing-fluid-induced formation damage by modeling the flow into a single hydraulic fracture in a shale gas reservoir. However, few studies discuss the efficient simulation methods and the impact of formation damage at the large SRV. In fact, the simulation of fracturing-induced formation damage in a scale of SRV generally requires a great number of gridblocks and consequently, a very large central processing unit (CPU) time, which makes the simulation prohibitive. In this paper, we focus our study on the hydraulic damage by simulating the full process of fracturing-fluid invasion followed by a cleanup of the loaded fluid in a complex fracture network within the entire SRV.

The necessity of full-field information for the hydraulically fractured well simulation has been discussed in the literature (e.g., Ehrl and Schueler 2000; Sadrpanah et al. 2006; Lolon et al. 2007; Fazelipour 2011; Delorme et al. 2013). In shale gas formations, it is important to take into account the presence of complex fracture networks, including stimulated and nonstimulated natural fractures, and their contribution to the gas production.

One of the critical issues in numerical modeling of shale gas reservoirs is how to handle fluid flows in the presence of a complex fracture network and the interaction between tight matrix formation and fractures **(Fig. 1).** Using a single-porosity model by explicitly discretizing fractures is a solution, but this approach needs a great number of cells and hence, a large CPU time. Cipolla et al. (2009) and Rubin (2010) propose to use an LS-LR-DK (logarithmically spaced, locally refined, and dual permeability) grid to reduce the number of cells with a single-porosity model. That technique uses large fracture cells (e.g., 2 ft in width) to mimic low-aperture fractures (e.g., 0.001 ft in aperture). Although equivalent large gridblocks can approximate gas production for single-phase flow, it is not adapted to simulate fracturing-fluid invasion with a two-phase-flow model, where water may invade into the matrix formation only several centimeters from the fracture face.

The DP model, where a shape factor is required to simulate the matrix–fracture interaction, is not suitable for shale gas simulations in general, because of the long transient flow period caused

This paper (SPE 173264) was accepted for presentation at the SPE Reservoir Simulation Symposium, Houston, 23–25 February 2015, and revised for publication. Original manuscript received for review 12 May 2015. Revised manuscript received for review 6 July 2016. Paper peer approved 8 July 2016.

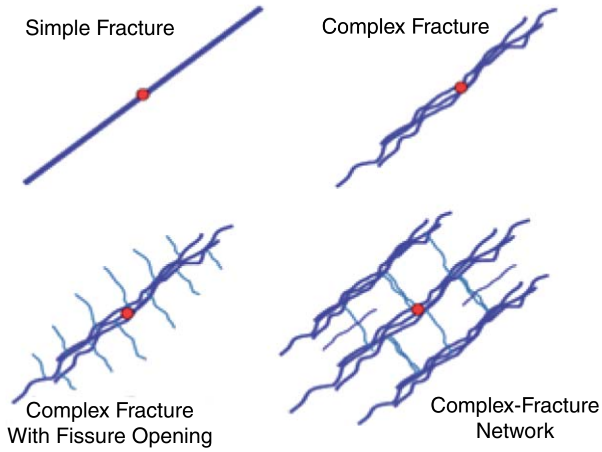

Fig. 1—Schematic of the level of hydraulic-fracture complexities (after Warpinski et al. 2008).

by large gridblock size with extremely low matrix permeability. To improve the simulation for matrix–fracture interaction, especially for multiphase-flow problems, the MINC approach (Pruess and Narasimhan 1983) seems to be a good alternative solution. The MINC method was used in many applications—for example, in the chemical enhanced-oil-recovery (EOR) processes (Farhadinia and Delshad 2010)—with satisfactory. Wu et al. (2013) also suggest to use the MINC approach for shale gas simulations. Here, we present a hybrid approach, on the basis of the MINC method, to simulate fracturing-fluid invasion and its backflow in shale gas reservoirs.

In this work, we only consider the hydraulic modeling of fracturing-fluid invasion without considering the geomechanical aspects of fracture generation. We assume that the fractures were already created, and that the width or aperture and the fracture permeability (or conductivity) are known. The fracture propagation is not explicitly considered. The leakoff during the fracturing is represented by injecting an appropriate volume of fluid into the formations. The hydraulic fractures and the reactivated natural fractures are considered fracture media for fluid transport, whereas the unstimulated natural fractures are homogenized in the matrix media. Interaction between matrix and fractures is modeled by use of very-fine nested submatrix blocks to ensure accurate calculation of water invasion and water-blocking effect caused by high capillary forces. This approach allows us to obtain almost the same results as an explicit discretized fracture model with a gain of an order of magnitude of 2 to 4 in CPU time. Therefore, the study of fracturing-induced formation damage and its impact on gas production can be achieved for the complex fracture network in an SRV in a shale gas reservoir with a reasonable CPU time.

Mathematical Model

Studying fracturing-fluid-induced formation damage requires simulating a multiphase-flow system. Here, we consider a two-phase flow in porous and fractured media, composed of nonmiscible gas and water phases. For simplicity, the gas and water components are assumed to be present only in their associated phases, and adsorbed gas is within the solid phase of rock. Each fluid phase flows in response to pressure and gravitational and capillary forces. Two mass-balance equations are needed to fully describe the system.

For a single-porosity two-phase-flow model, Eq. 1 alone is used for flow simulation in the whole reservoir, with different petrophysical properties for matrix and fracture media:

$$\frac{\partial}{\partial t}(\phi S_\beta \rho_\beta + m_g) + \mathrm{div}(\rho_\beta \vec{v}_\beta) - q_\beta = 0, \quad \ldots\ldots\ldots\ldots (1)$$

where subscript β represents phase with $\beta = g$ for gas and $\beta = w$ for water; ϕ is the porosity; S_β is the saturation of fluid β; ρ_β is the density of fluid β; $\vec{v}_\beta$ is the volumetric velocity vector of fluid β, determined by Darcy's law or non-Darcy flow models; t is time; m_g is the adsorption or desorption mass term for gas component per unit volume of formation; and q_β is the sink/source term of phase (component) β.

Furthermore, in a DP model, the mass conservation is applied to each phase β in both matrix and fracture media by the following equations:

$$\frac{\partial}{\partial t}(\phi^m S_\beta^m \rho_\beta^m + m_g) + \mathrm{div}(\rho_\beta^m \vec{v}_\beta^m) + Q_\beta^{mf} - q_\beta^m = 0, \quad \ldots\ldots (2)$$

$$\frac{\partial}{\partial t}(\phi^f S_\beta^f \rho_\beta^f) + \mathrm{div}(\rho_\beta^f \vec{v}_\beta^f) - Q_\beta^{mf} - q_\beta^f = 0, \quad \ldots\ldots\ldots\ldots (3)$$

where superscript m represents matrix media and f represents fracture media; and Q_β^m is the exchange term between the matrix and the fracture.

The phase velocity is expressed in both media with the Darcy equation:

$$\vec{v}_\beta = -K\frac{k_r\beta(S_\beta)}{\mu_\beta}\overrightarrow{\mathrm{grad}}(\Phi_\beta) \quad \text{with } \Phi_\beta = P_\beta + \rho\beta g Z_\beta = P_\beta + \rho\beta g Z, \quad \ldots\ldots\ldots\ldots (4)$$

where Φ_β is the potential of phase β; Z is depth; g is the algebraic value of gravitational acceleration; K is the absolute permeability of the medium; P_β is the pressure of phase β, μ_β is the viscosity of phase β; and $k_r\beta$ is the relative permeability to phase β.

For a DP model, the flow-exchange term between the matrix and the fracture is calculated by

$$Q_\beta^{mf} = \lambda_\beta^{mf}\sigma(\Phi_\beta^m - \Phi_\beta^f), \quad \ldots\ldots\ldots\ldots\ldots\ldots\ldots\ldots (5)$$

where, λ_β^{mf} is the mobility term to phase β; Φ_β^m and Φ_β^f are the potentials in the matrix and fracture media respectively; and σ is the shape factor, characterized by the matrix block geometry and matrix permeability under pseudosteady-state flow.

In addition, the term mg in Eqs. 1 and 2 is given by

$$m_g = \rho_r \rho_g V_E, \quad \ldots\ldots\ldots\ldots\ldots\ldots\ldots\ldots\ldots\ldots (6)$$

where m_g is the adsorbed gas mass per unit formation volume; ρ_r is rock bulk density; ρ_g is the gas density at standard condition; and V_E is the adsorption isotherm function or gas content in scf/ton (or standard gas volume adsorbed per unit rock mass). The system of equations (Eqs. 2 and 3) is discretized in space with a control-volume method, in which time discretization is carried out with a backward, first-order, fully implicit finite-difference scheme (see Appendix A).

MINC Method Concept

MINC was developed by Pruess and Karasaki (1982) and Pruess and Narasimhan (1983). Also, MINC is applicable to media where the fractures are well-connected (fracture network) so that a continuum treatment of flow in the fracture can be made. The MINC method is a generalization of the DP concept, originally developed by Barenblatt et al. (1960) and Warren and Root (1963); a schematic of the fluid-flow method in the DP model is given in **Fig. 2.**

Fluids in a fractured-porous medium will flow through the fractures to the well whereas matrix blocks can exchange fluid with the fractures. The main difference between the MINC method and a DP model is in handling matrix–fracture exchange known also by "interporosity flow." The DP method simulates matrix–fracture exchange on the basis of a pseudosteady-state flow, whereas the MINC method treats the problem entirely by numerical methods in a fully transient way. In other words, the interaction between matrix and fractures is treated by a fully transient representation.

The concept of the MINC method consists of partitioning matrix blocks into a sequence of nested volume elements, as

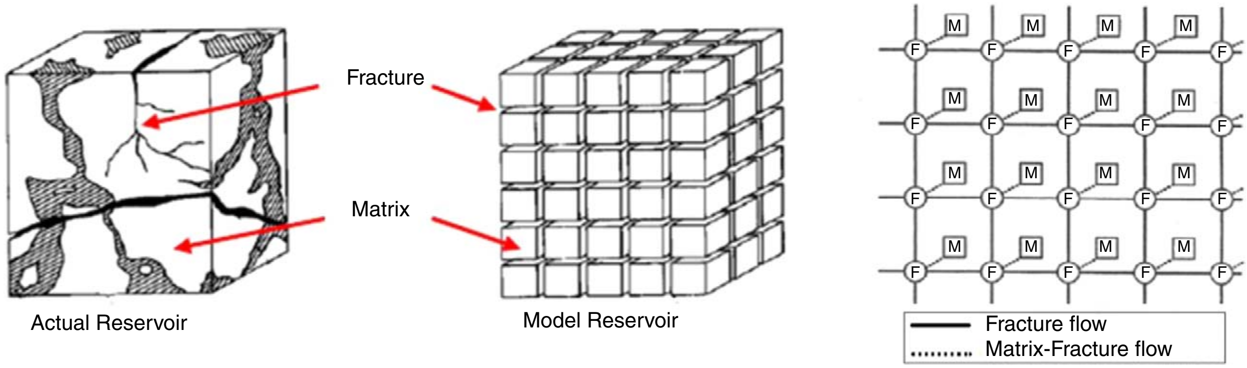

Fig. 2—Flow connections in the DP method (after Warren and Root 1963; Karsten Pruess 1992).

schematically shown in **Fig. 3** (left), where an MINC5 is presented, Continuum #1 represents the fracture, Continua #2, #3, #4, #5, and #6 represent the matrix media. Note that Fig. 3 (right) is a representation of MINC4, where 4 refers to the number of subdivisions in matrix media.

The MINC method presents a solution concerning the matrix–fracture flow exchange, which seems suitable and more accurate than a standard DP model. In addition, in case of multiphase (gas and water) flow simulations, very-fine subdivisions near the fracture are required to be a better simulation of the process of fluid invasion and fluid backflow after a hydraulic operation, which can be modeled accurately with the MINC method.

Furthermore, the application of the MINC method in partitioning matrix media into nested cells on the basis of the distance from the fracture is not limited to a regular fractured network, but can also be applied to an irregular network.

Hybrid Approach Based on the MINC Concept

In general, unconventional gas reservoirs are naturally fractured, which increases difficulty and complexity of reservoir simulations. The most commonly used numerical methods for flow simulations in this kind of reservoir are based on single-porosity or DP models. Unstimulated natural fractures are homogenized and considered as a part of media. Simulations with explicitly discretized fractures with very-fine gridblocks as fracture width with a single-porosity approach can give us a very-accurate flow modeling into and from fractures, especially for two-phase flow problems. Advanced numerical methods are also studied in the literature to improve discrete fracture modeling for multiphase/multicomponent flows (e.g., Geiger et al. 2009; Schmid et al. 2013; Zidane and Firoozabadi 2014). However, an explicitly discrete fracture model (DFM) involves a large number of cells which are not suitable for reservoir-scale simulations because of the computational intensity. Moreover, the commonly used DP approaches that are based on pseudosteady-state flow regime are often inadequate for solving long-lasting transient fluid flow from such reservoirs where the main problem is that we are dealing with tight reservoir rock with nanodarcy permeability.

In this paper, we will present a hybrid modeling approach that is based on the concept of the MINC method. The MINC approach was investigated by Ding et al. (2014) for the single-phase flow simulation in shale gas reservoirs. The purpose of this paper is to improve the two-phase-flow simulation model by means of the matrix–fracture interaction in extremely low-permeability fractured reservoirs with the MINC method. This approach exists in a hybrid discretization logarithmically spaced near fractures. Furthermore, our study focuses on the impact of hydraulic damage caused by fracturing-fluid invasion into the tight formation by simulating the entire process of the fracturing operation in a complex fracture network from shale gas reservoirs.

We will also present the benefits of using the hybrid approach based on the concept of the MINC method. First, this approach reduces the number of grid cells, which obviously could result in decrease in computational time. In fact, a flow simulation with this approach takes seconds or minutes rather than hours or days compared with an explicit discretized model on the same hardware. Second, this approach is accurate. We will show some comparisons with the reference solutions (extremely refined grid with explicit fracture discretizations) for different fracture spacing. In addition, various physical processes could be tested with this hybrid model (for example, adsorption/desorption, geomechanics, Klinkenberg aspect).

The purpose of this hybrid method is to improve matrix–fracture flow simulation. On the basis of the MINC approach, matrix media are subdivided into several nested volumes, which look

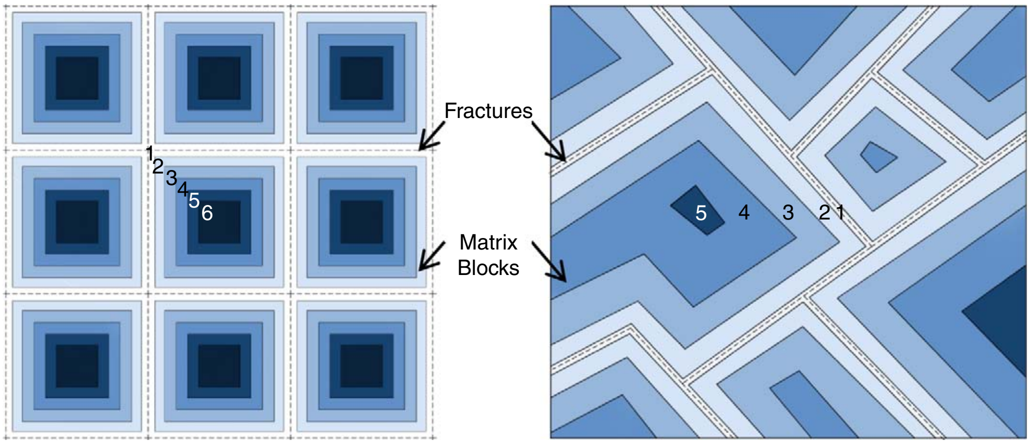

Fig. 3—Schematic of MINC concept: (left) for a regular fractures network (after Pruess and Narasimham 1983), (right) for an arbitrary fractures distribution (after Pruess and Karasaki 1982; Pruess 1992).

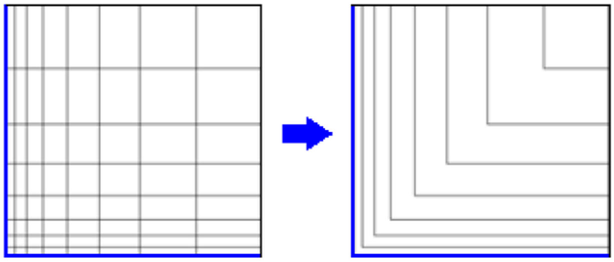

Fig. 4—The 2D fracture model, discretized model (left), and its MINC optimization with nested subgrids (right).

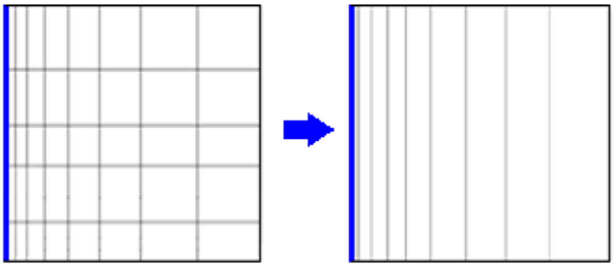

Fig. 5—The 1D fracture model in *y*-direction and its optimization with the MINC method.

Property/Parameter	Value
Matrix Permeability	0.0001 md
Hydraulic-Fracture Permeability (during hydraulic fracturing)	200 darcies
Hydraulic-Fracture Permeability (during production)	2 darcies
Induced-Fracture Permeability (during hydraulic fracturing)	40 darcies
Induced-Fracture Permeability (during production)	0.5 darcies
Matrix Porosity	5%
Fracture Porosity	50%
Fracture Thickness	0.01 ft
Induced-Fracture Thickness	0.001 ft
Reservoir Net Thickness	300 ft
Top of the Reservoir	5,800 ft
Initial Reservoir Pressure	3,800 psi
Bottomhole Well Pressure	1,000 psi

Table 1—Reservoir properties.

more suitable than a DP/permeability model and can handle the physics of such flow. Note that the MINC concept could be a solution of the interporosity flow, where this approach can treat this problem entirely by a fully transient representation of matrix–fracture flow. We assume that the stimulated fracture network can be represented by regular fracture geometry with a uniform spacing in the SRV. So, we use a standard MINC method inside SRV, and single-porosity approach in the nonstimulated zone. In the transient zone between SRV and nonstimulated volume, we use a generalized MINC approach with nested fine cells around the fracture, as shown in **Fig. 4 and Fig. 5.**

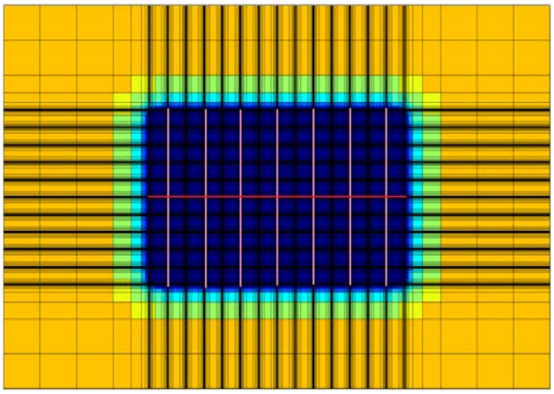

Fig. 6—Explicit discretized fracture model with a horizontal well for Case 1.

Moreover, to correctly simulate fracturing-fluid invasion and its backflow, very fine cells should be used near the fractures for fracture–matrix interaction simulations because fluid invasion is generally not deep into the tight formation. Fluid transport should be considered in the multiscale fracture network. This hybrid approach that is based on the concept of the MINC method for a multiphase flow will be tested on a synthetic reservoir example, to show if it is able to handle the physics of such flow by comparing it to an explicit discretized and a standard DP model.

Numerical Examples

To study the impact of fracturing-fluid-induced formation damage in shale gas reservoirs, simulations for a single-phase (gas only) flow were first performed to test the effectiveness of our approach that is based on the concept of the MINC method. After this approach is tested, a two-phase (gas and water) flow simulation will be performed to quantify the impact of formation damage on gas production from shale gas reservoirs.

Table 1 summarizes the reservoir properties. A horizontal well (red line in **Fig. 6**) in the *x*-direction is placed in the middle of the reservoir, where hydraulic fractures are perpendicular to the well along the *y*-direction. Note that, two areas exist in the reservoir model, the first one known as SRV and the other as non-SRV. The SRV has a volume of $1{,}400 \times 1{,}000 \times 300$ ft^3 and is centered in the model.

On the one hand, a base-case model named "explicit discretized model" (or single-porosity model), meshed with a local grid refinement around the stimulated fractures, logarithmically spaced, is considered a reference solution. Our reservoir model presents

Case	Fracture Spacing	Number of HF	Number of NFx (stimulated fractures parallel to the well direction)	Number of NFy (stimulated fractures perpendicular to the well direction)
Case 1	100 ft	7	11	8
Case 2	50 ft	7	21	22
Case 3	25 ft	7	41	50

Table 2—Representation of HF (hydraulic fractures), NFx and NFy (stimulated fractures in x- and y-direction), for the three considered cases.

different scale fractures in the x- and y-direction dedicated to hydraulic and induced fractures, where grids dedicated to the hydraulic fractures in the y-direction have a width of 0.01 ft, a permeability of 2,000 md (during production), whereas the stimulated natural fractures are presented in the x- and y-direction with a thickness of 0.001 ft and a permeability of 500 md (during production). On the other hand, the DP model consists of two interconnected media, named matrix and fracture. For the DP model, the gridblock size is 200 ft in the x- and y-direction. Comparisons are made between the reference solution and DP/hybrid approach. Care was taken to be consistent in the calculation of the effective fracture permeability and porosity for the DP model, where the shape factor σ for calculating matrix–fracture exchange is given by

$$\sigma = \frac{10}{a^2} + \frac{10}{b^2}, \quad \text{(7)}$$

where a and b are the matrix block dimensions (in the x- and y-direction).

First, single-phase flow is treated. Later, the two-phase (gas and water) flow problem is considered to simulate fracturing-induced formation damage. We assume that the hydraulic fractures have already been created, and we do not consider the geomechanics effects in our simulations. Three cases are considered for different fracture spacing. **Table 2** summarizes these three cases.

In all cases, 7 hydraulic fractures perpendicular to the well direction are created. Inside the SRV zone, for Case 1, the induced/stimulated fractures can be approximated by a fracture network with a spacing of 100 feet in the x- and y-direction. This network is schematically represented in Fig. 6 by 15 fractures (7 hydraulic and 8 induced fractures) in the y-direction and 11 induced fractures in the x-direction. For Case 2, 7 hydraulic fractures in addition to 22 induced fractures in y-direction with a spacing of 50 feet and 21 reactivated fractures in the x-direction are created. Finally, for Case 3, 57 fractures (7 hydraulic and 50 induced fractures) in the y-direction and 41 induced-fractures in the x-direction with a spacing of 25 ft are incorporated. Outside the SRV, no stimulated fractures are considered. The total stimulated area is 1,000 ft in y-direction and 1,400 ft in the x-direction.

Fig. 6 and **Fig. 7** represent the grid system used for the explicit discretized fracture model for Case 1 (fracture spacing of 100 feet) and the standard DP model. **Fig. 8** is a schematic of the hybrid approach that is based on the MINC method for the same reservoir.

Simulation Results

In this session, single-/two-phase flow-simulation results are presented. In the single-phase flow simulation, formation damage related to the fracturing-fluid invasion is not considered to test the efficiency of our hybrid approach. We assume that gas is the only mobile phase in the reservoir and will be directly produced from the complex fracture network. Then, simulations are performed with a two-phase (gas and water) flow model to study the impact of the fracturing-fluid-induced formation damage in shale gas reservoirs.

Single-Phase Flow-Simulations. First, this study concerns only Case 1 to show the efficiency of the hybrid method by plotting different refinement. For example, **Fig. 9** shows the convergence of the cumulative gas production for different hybrid-approach model (MINC2, MINC4, MINC6, and MINC14) compared with the explicit discretized model, which is considered a reference solution. Fig. 9 (left) describes the cumulative gas production for 5,000 days, where Fig. 9 (right) presents the cumulative curves for 1,000 days of production. On the one hand, increasing the order of refinement for the hybrid approach improves the gas production and makes the result more accurate. However, with a MINC6 or MINC14 model gave us nearly the same results which are very accurate compared with the reference solution. On the other hand, it is clear that, beyond a MINC6, there is no more need to refine, and a MINC6 model is sufficient for a single-phase-flow case.

Fig. 10 presents the L_2 norm error function of number of refinement with a semilog concerning the norm error Y-axis for a single-phase flow-simulation. The L_2 norm error is defined as:

$$L_2 = \sqrt{\frac{1}{N}\sum_{i=1}^{N}\varepsilon_i^2} \quad \text{(8)}$$

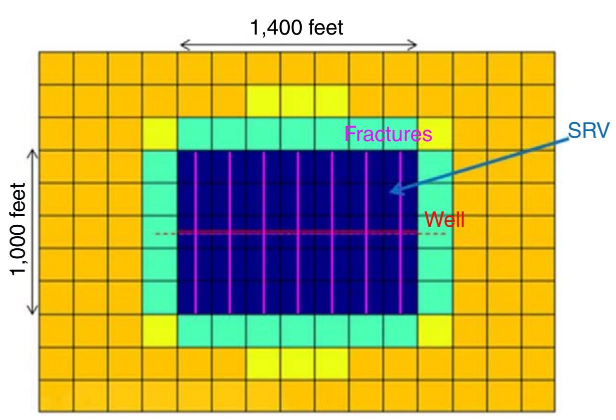

Fig. 7—DP model for Case 1 (fracture spacing of 100 ft).

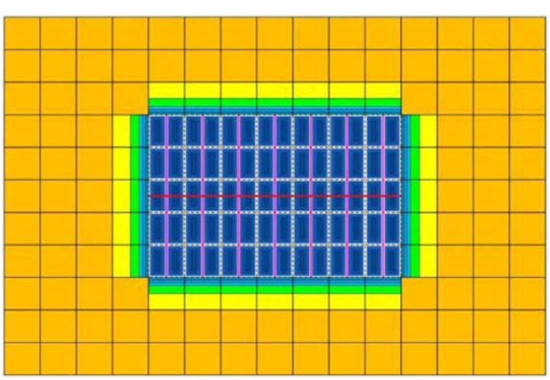

Fig. 8—Hybrid-approach model that is based on the MINC method for Case 1.

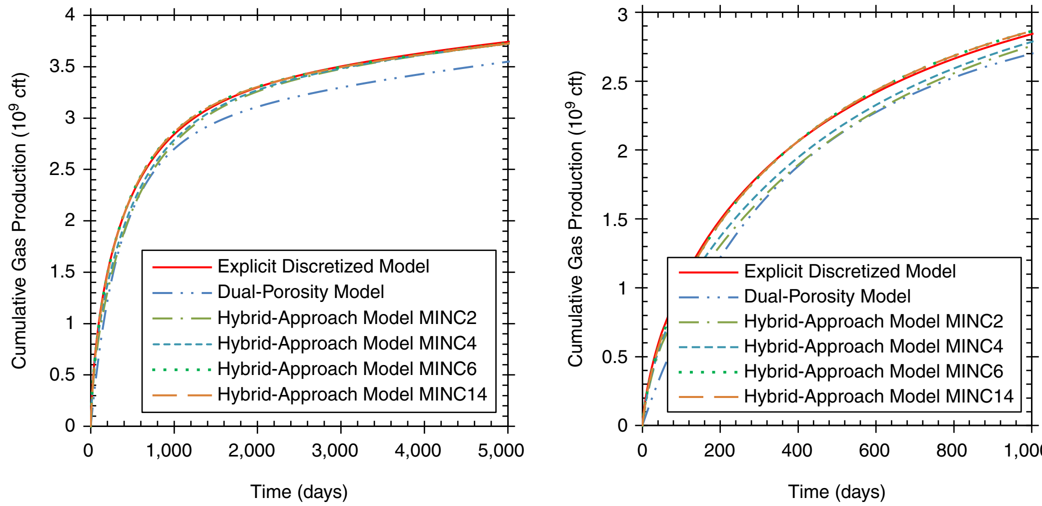

Fig. 9—Comparison of different order of refinement for the MINC method to the reference solution and the DP model for 5,000 days (left) and 1,000 days (right) for Case 1.

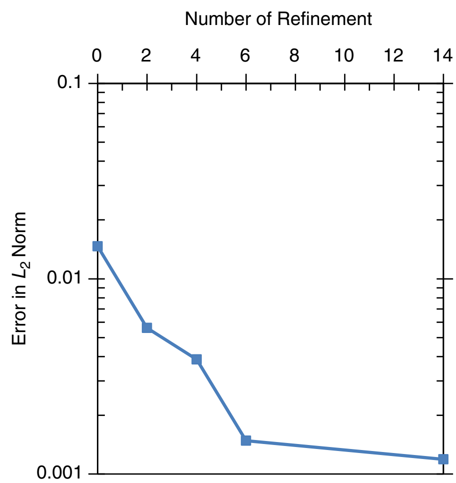

Fig. 10—The L_2 norm error function of number of refinement concerning a single-phase flow for the cumulative gas production for Case 1.

where N refers to the number of points in the calculation, ε represents the difference between the hybrid approach and the reference solution, and i corresponds to the time index. In our case, $N = 100$.

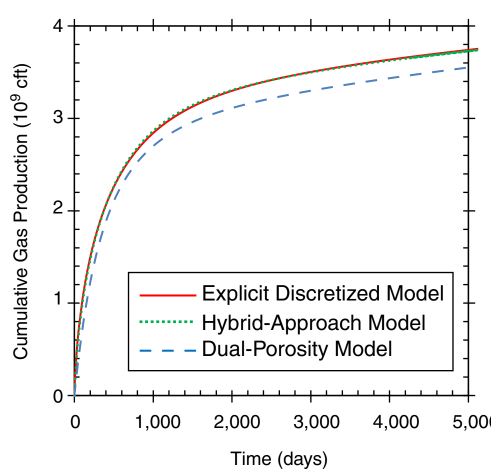

Fig. 12—Comparison of different simulation models for Case 2.

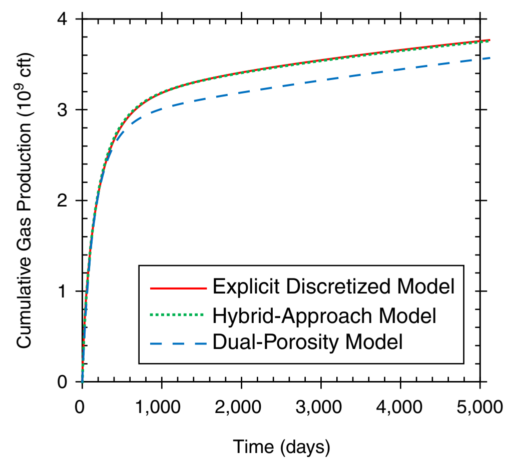

Fig. 11—Comparison of different simulation models for Case 1.

This study has been performed on the cumulative gas production for Case 1. On the basis of the results from the norm error as a function of the number of refinement, we consider that using MINC6 is sufficiently accurate for single-phase flow simulations.

Three simulation models (explicit discretized model, DP, and hybrid approach) are compared for Case 1 and Case 2. For the hybrid approach, MINC6 model (1 continuum for the fracture and 6 continuums for the matrix medium) is used in the SRV. **Fig. 11** presents the cumulative gas production for Case 1 (fracture spacing of 100 ft) after 5,000 days of production performed with these three simulation models. Obviously, the hybrid approach that is based on the concept of the MINC method provides a much better result than the DP model and can match accurately the explicit discretized fracture model (reference solution). **Fig. 12** shows the results of cumulative gas production for Case 2 (fracture spacing of 50 ft). We get the same conclusions as for Case 1. The hybrid approach works very well independently from fracture spacing (100 and 50 ft). These simulations show that the hybrid approach can predict gas production from unconventional fractured gas reservoirs. This hybrid technique with many fewer gridblocks can simulate single-phase flow problems with a good accuracy. Because the hybrid approach is quite accurate, to investigate the impact of fracture spacing on gas production from shale gas reservoirs, Case 3 (fracture spacing of 25 ft) was simulated with the hybrid model only. Note that, simulation of Case 3 with an explicit discretized fracture model was avoided with the hybrid approach, where an explicit discretized fracture simulation could

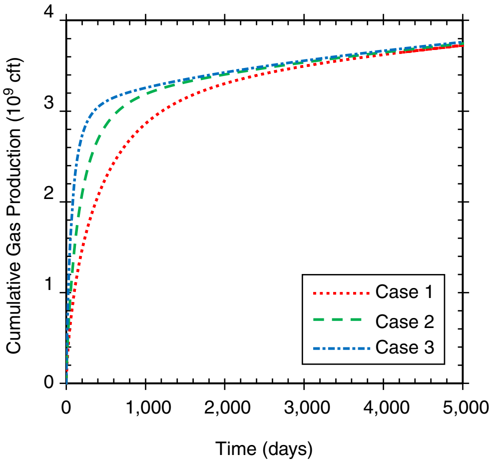

Fig. 13—Comparison of the hybrid-approach results for different fracture spacings (Case 1, Case 2, and Case 3).

take several hours rather than seconds because of the large number of grid cells. **Fig. 13** shows the difference of cumulative gas production from these three cases by use of a hybrid-approach model for the single-phase-flow simulation. In fact, decreasing the fracture spacing increases fracture numbers which results in enhancing gas production. As we expected, the higher gas production is observed in Fig. 13 for Case 3 than for Case 2 and Case 1. Simulation with a hybrid approach with a MINC6 model for the entire SRV seems to be sufficiently accurate and computationally efficient for a single-phase flow simulation.

On the basis of these results for the single-phase flow problem, we conclude that the standard DP model is not suitable for shale gas simulations, and the hybrid model is a good approach. The hybrid model with the MINC technique proves its accuracy for the application on shale gas reservoir simulation. In addition, the MINC method significantly improves the capability to predict matrix–fracture flow, where discretizing the matrix blocks into a sequence of volume elements can handle much better the transient flow from matrix into fracture during a long transient period instead of pseudosteady-state flow with the standard DP model.

Two-Phase Flow-Simulations. To improve gas production from shale gas reservoirs, hydraulic fracturing operations are required. With hydraulic fracturing, a huge amount of water (thousands of barrels) is injected to create multistage hydraulic fractures for the purpose of obtaining an economic production from unconventional gas reservoirs. We should mention that only a fraction of the injected water (25–60%) is reproduced during a long-period backflow and production, while a significant percentage of water remains in the reservoir, trapped in rock matrix near the fracture face caused by capillary effects.

With the two-phase-flow model, water is first injected during hydraulic fracturing. Because of injection pressure and capillary forces, water will invade into the matrix formation. In this example, a volume of 25,000 bbl of water is pumped into the horizontal fractured well (seven fracture stages) in 5 hours. During hydraulic fracturing, fracture conductivity is usually very high because if high-fracturing pressure. So, during the fracturing phase, the permeability is assumed to be 200 darcies in the hydraulic fractures and 40 darcies in the stimulated natural fractures. During the production phase, the permeability is decreased to 2 darcies in the hydraulic fractures and 500 md in the stimulated natural fractures.

Both gas/water relative permeabilities in matrix and fracture media, together with the capillary pressure, are needed to be incorporated in the reservoir model for the two-phase-flow simulation. **Figs. 14 and 15** show, respectively, matrix/fracture relative permeabilities and the capillary pressures vs. water saturation. Furthermore, we consider that the initial water saturation in this shale gas reservoir equals the irreducible water saturation, set at 0.35.

In dealing with two-phase-flow simulation, the MINC6 model was found to be insufficient to handle fluid invasion and its backflow, because we need several very small gridblocks around the fractures to correctly simulate water invasion in the matrix formation. To improve our model results for the two-phase-flow simulation, we decided to increase the number of nested volumes related to the matrix media, with a MINC13 model (1 continuum for the fracture and 13 continuums for the matrix medium) instead of a MINC6 model (single-phase case).

In fact, to select a reasonable MINC for two-phase flow simulations, we performed several MINC tests for Case 1, where 100 ft of fracture spacing is considered. The convergence of the two-phase-flow simulation with different MINC refinement (MINC 4, 8, 10, 13, and 14) is presented in **Fig. 16.** It is obvious that, by adding supplement continuum from 4 through 8 to 10 through 13, the results of cumulative gas production are more accurate. It should be mentioned that beyond MINC13 there is no need to refine more. Clearly, MINC14 provides nearly the same result of MINC13.

This claim could be explained on the basis of the results of the L_2 norm. **Fig. 17** presents the L_2 norm error function of different number of refinement for the cumulative gas production (left) and for the cumulative water production (right) concerning a two-phase flow for Case 1, respectively. Clearly, the L_2 norm error is decreasing by increasing the number of matrix subdivision, and a MINC13 model is sufficiently accurate for this simulation case.

Case 1—Fracture Spacing of 100 ft. Considering Case 1, simulation results from fracture spacing of 100 ft are presented in **Fig. 18.** The results from the DP model and hybrid approach are

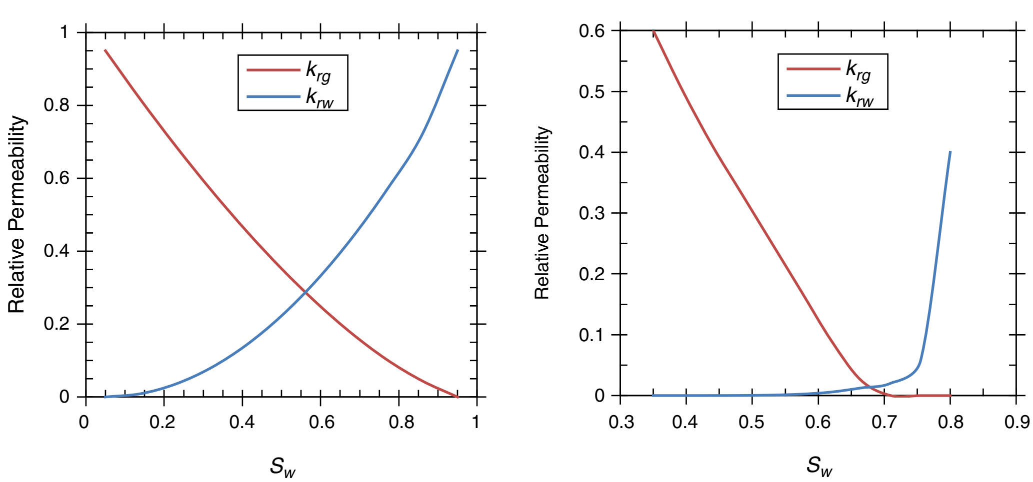

Fig. 14—Fracture relative permeability curves (left) and matrix relative permeability curves (right) vs. water saturation.

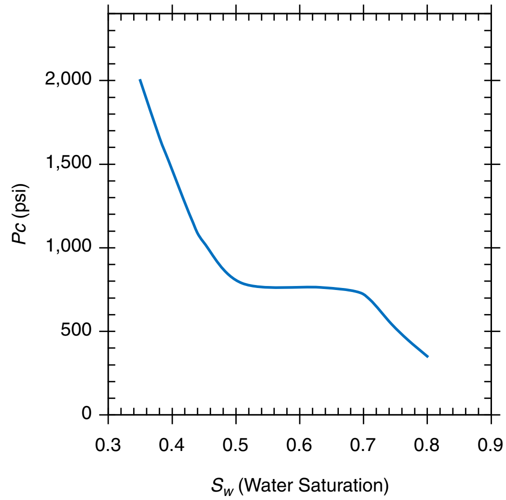

Fig. 15—Capillary pressures vs. water saturation.

compared with the explicitly discretized fracture simulation (reference solution). Figs. 18a, 18b, 18c, and 18d represent, respectively, the results of daily water rate, daily gas rate, cumulative water production, and cumulative gas production for this two-phase flow simulation for the same reservoir model, as defined previously (see Fig. 6, Fig. 7, and Fig. 8).

Fig. 18b shows the daily gas rate during the first 1,000 days. The gas rate is affected by the presence of fracturing fluid during the cleanup period. Although the hybrid method is not very accurate in the very early time, it is much better than the DP model. This approach gives reasonable and satisfactory results to predict well productions. Fig. 18c presents the simulated water-production curves in the first 100 days. The explicit discretized model and the hybrid MINC approach (dotted green curve) produce approximately 8,000 bbl of water in 100 days, whereas the DP model produces close to 9,000 bbl. In fact, approximately 30% of injected water is produced, and the rest of the water remains in the tight formation and needs a very long time to be cleaned out. The hybrid approach gives a similar water production as the explicit discretized model, whereas the DP model overestimates the production rate.

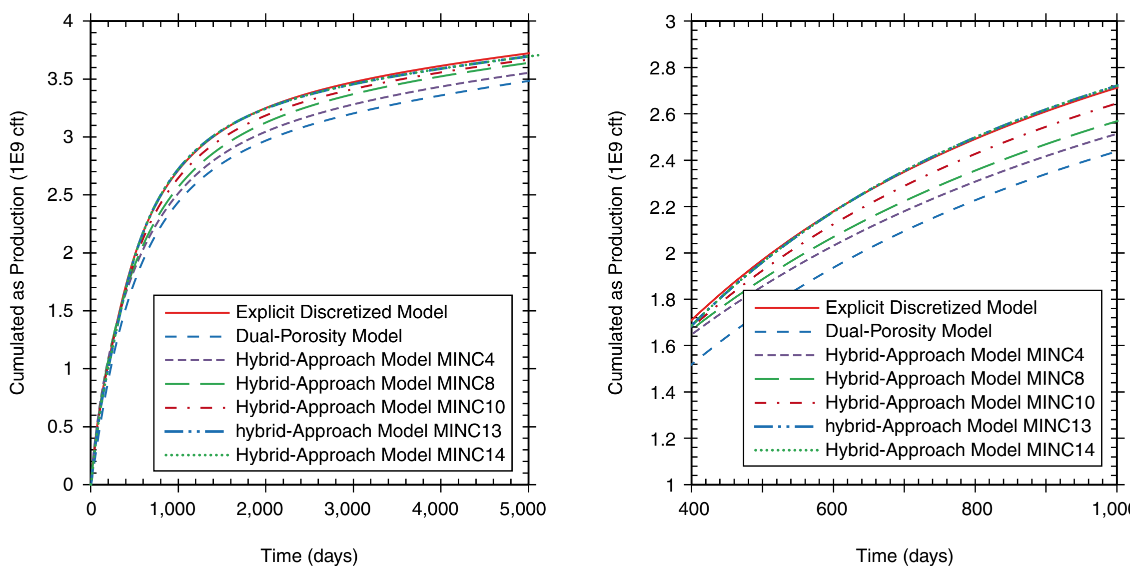

Fig. 16—Comparison of different order of refinement for the MINC method to the reference solution and the DP model for 5,000 days (left) and from 400 to 1,000 days (right) for Case 1.

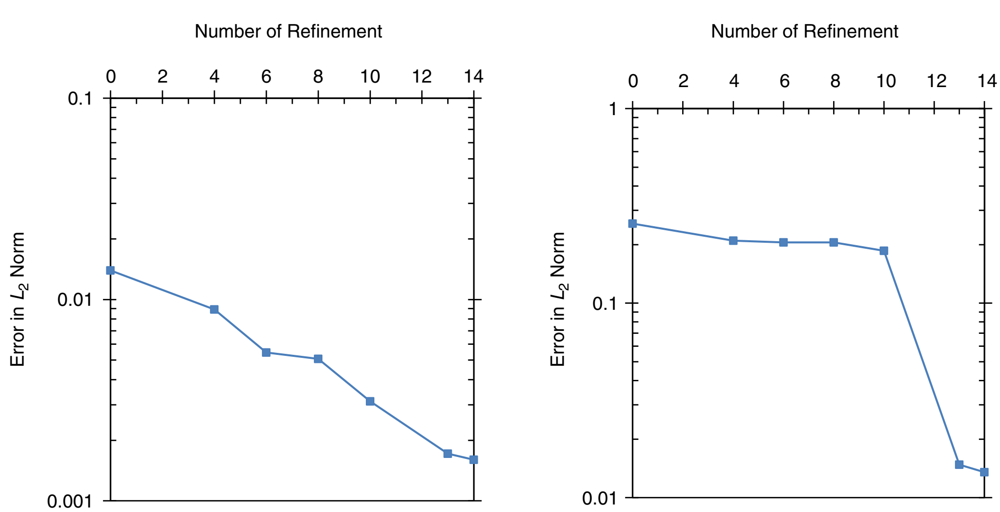

Fig. 17—The L_2 norm error function of number of refinement concerning a two-phase-flow for the cumulative gas production (left) and the cumulative water production (right) for Case 1.

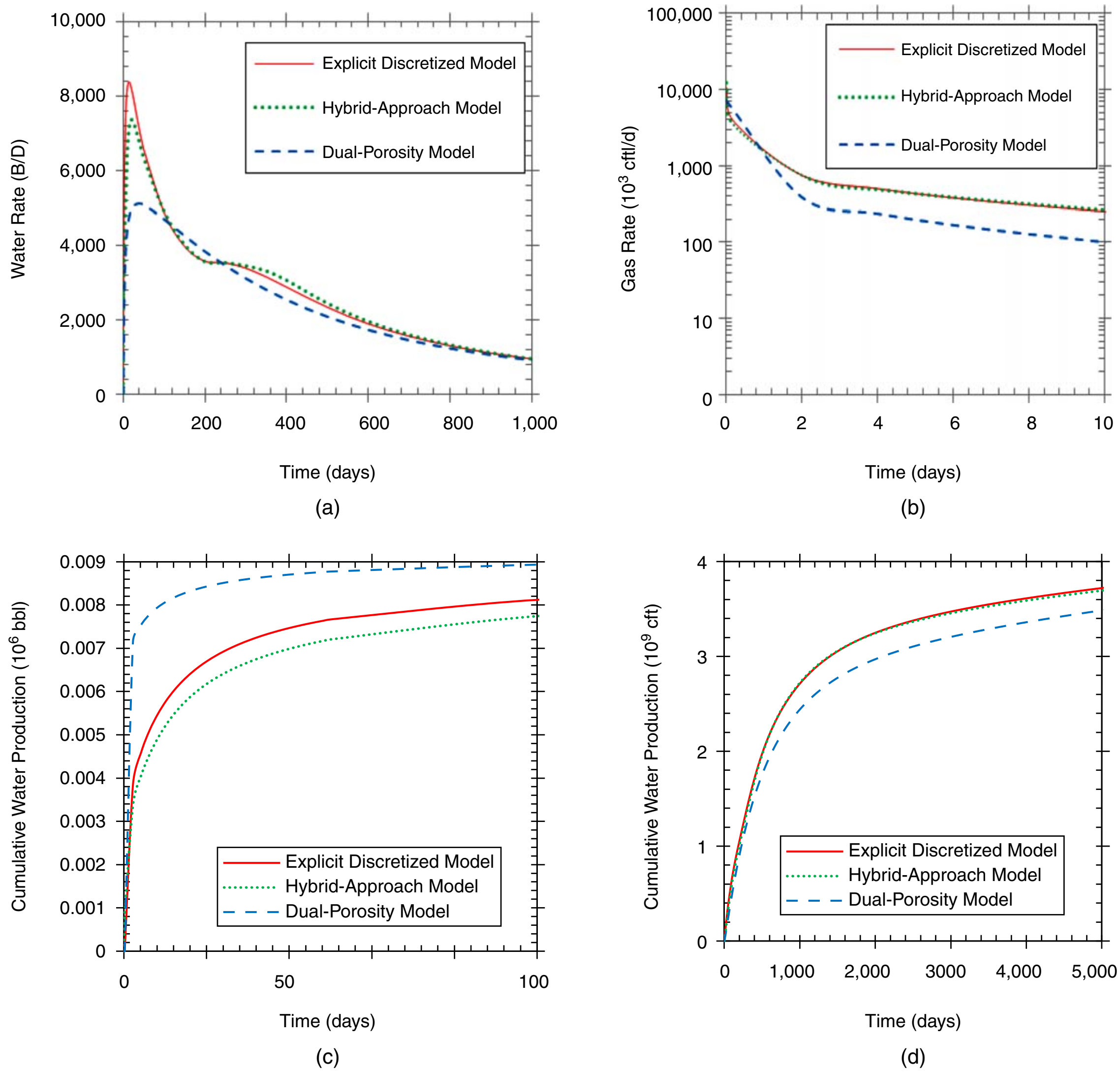

Fig. 18—Comparison of different simulation-model results for Case 1 for a two-phase flow case. (a) Daily water production vs. time. (b) Daily gas rate vs. time. (c) Cumulative water production vs. time. (d) Cumulative gas production vs. time.

If we are interested in long-term production, on the basis of Fig. 18d, which presents the cumulative gas production for 5,000 days, the hybrid method is very accurate and the DP model still not suitable.

Case 2—Fracture Spacing of 50 ft. The following simulations are carried out for the fracture spacing of 50 ft. Results are presented in **Fig. 19.** Figs. 19a, 19b, 19c, and 19d represent, respectively, the results of daily water rate, daily gas rate, cumulative water production, and cumulative gas production. The daily water rate for the first 10 days is presented in Fig. 19a. The cumulative water production during the first 100 days is shown in Fig. 19c. In this case, water production is reduced to 6,500 bbl by the explicit discretized model and the hybrid approach. In fact, this is because the total fracture length is longer in Case 2 than in Case 1 where smaller fracture spacing is treated and then obviously larger fracture–matrix interface will be per unit volume of formation. So, little water invades the matrix formation per unit of fracture surface. It is more difficult to remove a small quantity of water, because of the water-blocking effect and the high capillary pressure (2,000 psi). In other words, decreasing the fracture spacing increases the number of fractures or the exchange surface with the matrix medium. Therefore, the water invasion is extended to a very larger area, and the water backflow is reduced. The produced water from Case 2 corresponds to 25% of injected water. The hybrid simulation in this case is more accurate than the previous case (fracture spacing of 100 ft). This is because the water invasion in this case is shallow in the matrix formation, and MINC13's mesh is sufficiently fine around the fracture to simulate this water invasion. Moreover, the shorter transient period because of small block sizes also helps to improve the MINC simulation accuracy. On the contrary, the DP model highly overestimates the water production and is not accurate. Fig. 19b presents the daily gas rate in early time, and Fig. 19d shows the accumulation of gas production for 5,000 days. The hybrid method is very accurate in both early and later times. The DP model is always not accurate.

The simulations of these two cases (fracture spacing of 100 and 50 ft) allow us to confirm that the hybrid approach is accurate and can be used as a reference solution for further simulations. The hybrid approach can be used to simulate matrix-fracture exchange even for a multiphase flow case independently from fracture spacing (Case 1 and Case 2). It has to be mentioned that our simulation results from daily water and daily gas production have been compared with data from Marcellus shale gas wells at early time (e.g., see Cheng 2012; Clarkson and Williams-Kovacs 2012). Hereafter, the simulation results from daily water and gas rate are presented in log-log scale to compare them to data from Marcellus Field (Cheng 2012). The water productions are compared during the cleanup period in the very early time. **Fig. 20** presents the daily water rate from Case 2 (left) for the first 20 days and from the Marcellus Field. At the beginning, we have a water production approximately 2,000 B/D, and it is reduced to

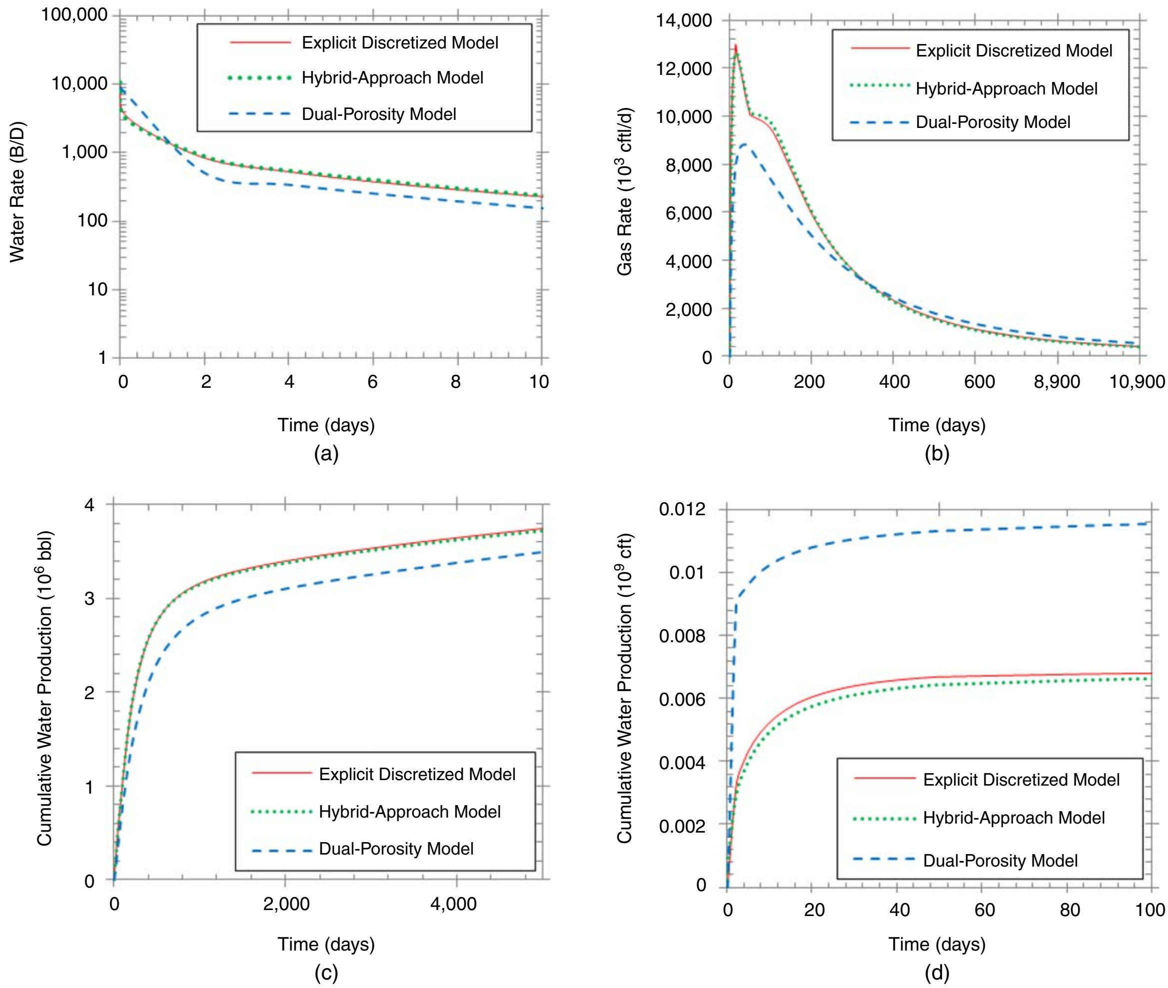

Fig. 19—Comparison of different simulation-model results for Case 2 for a two-phase-flow case. (a) Daily water rate vs. time. (b) Daily gas rate vs. time. (c) Cumulative water production vs. time. (d) Cumulative gas production vs. time.

100 B/D at the end of 20 days. Our daily water production presents a similar trend compared with that from the Marcellus Field in the cleanup period. **Fig. 21** presents the comparison concerning the daily gas rate from Case 2 and Marcellus Field. The gas production in Case 2 starts from 10,000 B/D and decreases to approximately 500 B/D at 1,000 days. Although our simulation shows quick decline because of small SRV, it presents similar trends as the field data.

In the following, we will use the hybrid method as the reference solution to simulate the case of fracture spacing of 25 ft to investigate the effect of formation damage.

Impact of Fracturing-Fluid-Induced Formation Damage. Because of the high capillary force, water-based fracturing fluid will invade through matrix media. Then, water is trapped in the tight formation, and only a fraction of the injected water can be produced. Unproduced or trapped water will lead to a blocking

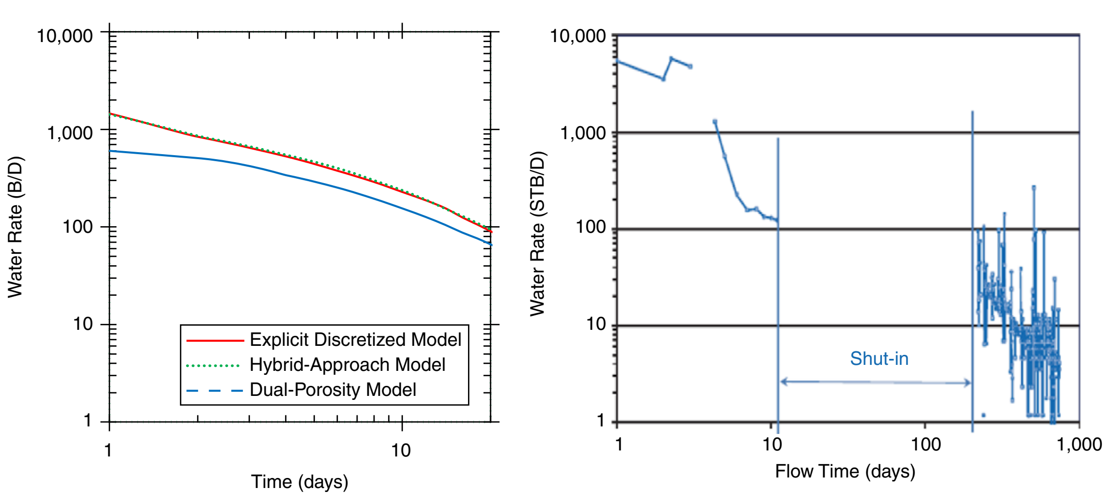

Fig. 20—The daily water-rate production from our case (left) and from the Marcellus case (right, from Cheng 2012).

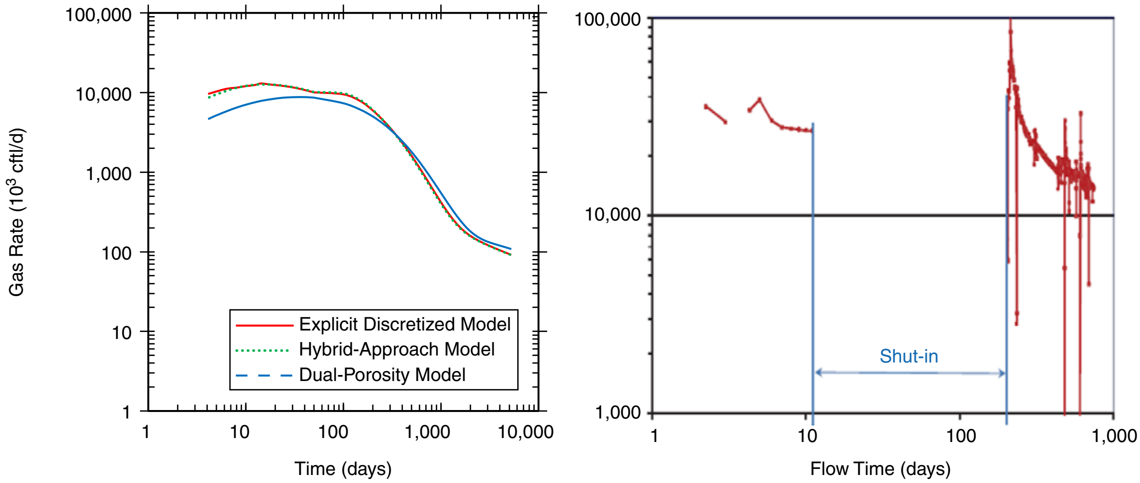

Fig. 21—The daily gas-rate production from our case (left) and from the Marcellus case (right, from Cheng 2012).

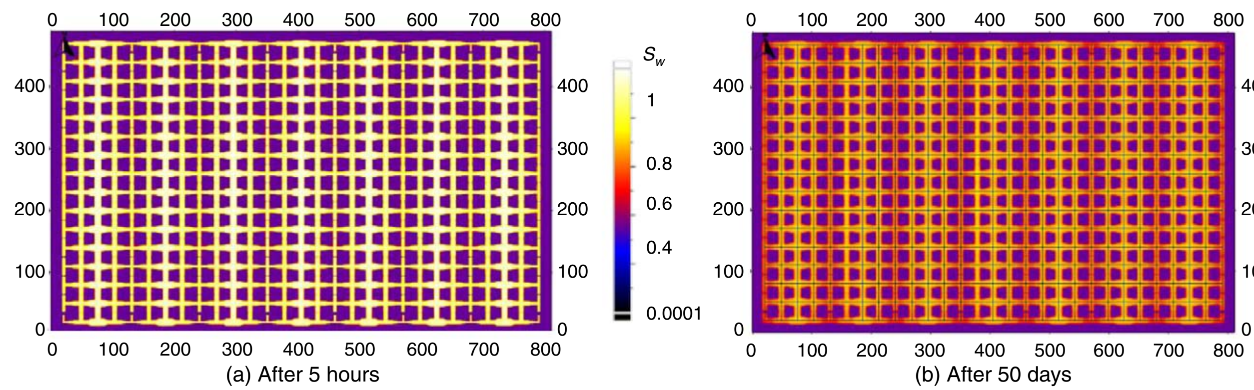

Fig. 22—Water-saturation distribution (fracture Spacing of 50 ft).

effect in the matrix formation caused by high capillary pressures and water-sensitive clays. The presence of water will unfortunately reduce effective gas permeability, and may impact gas production from shale gas reservoirs.

To illustrate the impact of water invasion, **Fig. 22** shows some illustrative figures for the fracture spacing of 50 ft (Case 2), where

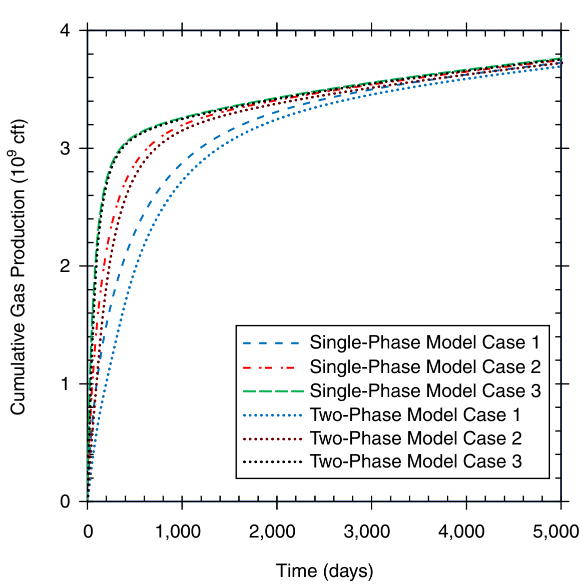

Fig. 23—Impact of water invasion on gas production for Case 1, Case 2, and Case 3.

the cells near the fractures are zoomed. In these figures, water saturations inside and near fracture cells are illustrated at the end of injection (after 5 hours) and at the 50th day of production. After 5 hours of water injection, fracturing fluid invades approximately 0.15 ft into the matrix formation. After 50 days of gas production, water saturation is still approximately 0.65–0.75 in the tight formation near the fracture faces. A lot of time is needed to clean out the invaded water.

In this section, we will study the impact of fracturing-fluid-induced formation damage by comparing the single-phase flow simulation, where no formation damage is considered, and the two-phase flow simulation, where the formation damage caused by fracturing-fluid invasion is taken into account. **Fig. 23** presents these comparisons for fracture spacing of 100, 50, and 25 ft (Case 1, Case 2, and Case 3), respectively. We notice that gas productions from single-phase flow simulations (no formation damage) are higher than those from two-phase flow simulations (fracturing-induced formation damage), because of capillary trapping, and others. This methodology can be used to evaluate quantitatively the effect of fracturing-fluid-induced formation damage.

The formation damage for Case 1 is more important than Case 2 at earlier time of production, while it can almost be neglected in Case 3. In fact, we can notice that the formation damage becomes less important when the number of fractures increases (decreasing the fracture spacing). This result can be explained by the formation damage through water-invasion depth. In fact, when fractures are dense, the volume of water invasion into the matrix formation by unit fracture surface becomes small. After the fluid invasion is shallow, the impact of water invasion on gas production will be insignificant. This claim can be explained by **Fig. 24.** In Fig. 24, the water saturation near the fractures as a function of the distance from the fractures is plotted for Case 1, 2, and 3. Clearly, the

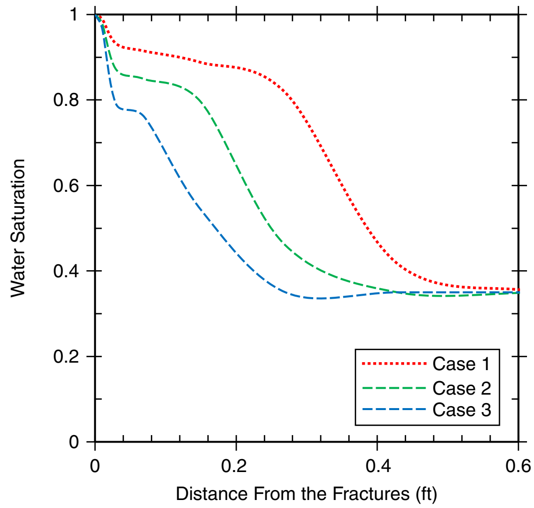

Fig. 24—Water saturation around the fractures for Case 1, Case 2, and Case 3.

formation for Case 1 is more damaged than Case 2 and Case 3, and it explains the impact on the cumulative gas production in Fig. 23.

A summary of numerical-simulation results is presented in **Table 3**, which includes the number of gridblocks, CPU times, average water-invasion depth, and the smallest gridblock volume. Table 3 compares the CPU times between the explicit discretized fracture model and the hybrid approach for single- and two-phase-flow simulations of each case. For the single-phase-flow simulations, an explicitly discretized fracture model took 2 hours and 8 hours, respectively, for Case 1 and Case 2, whereas for the hybrid model with MINC6 which uses only 1,039 gridblocks, an average of 8 seconds of CPU time was used in the simulation for each case independently from the fracture spacing. It has to be mentioned that Case 3 was not simulated with an explicit discretized model because of the high number of grids cells (1.5 million grids approximately). Furthermore, concerning the two-phase-flow simulations, an enormous CPU time is required with the explicit discretized fracture model (more than 5 hours and 24 hours, respectively for Case 1 and Case 2). The hybrid approach is much more-efficient and faster than the explicitly discretized model. The CPU time is reduced to 12 seconds for all the three cases with a MINC13 model (1,529 meshes for a two-phase-flow simulation independently from fracture spacing). This approach decreases significantly the number of meshes and the CPU time compared with an explicit discretized model. Also, the accuracy of the MINC method does not depend on the fracture spacing.

It is clear that an explicit discretized model takes great amount of computational effort. The large number of gridblocks required in an explicitly discretized model increases the CPU time in solving the system at each timestep, and also the small volume of the gridblocks constrains the timesteps (need to use very small timesteps). Table 3 also presents the smallest grid volume for each case for different simulation models. It is shown the smallest block volume for the hybrid approach is 6 orders of magnitude greater than that of the explicit-fracture discretization model (0.0003 ft^3 for the explicit discretized model and 120, 240, and 480 ft^3, respectively, for Cases 1, 2, and 3). The explicitly discretized model is greatly penalized in CPU time, especially for two-phase flow problems.

Concerning the depth of fracturing-fluid invasion, it is 0.27 ft for the large fracture spacing of 100 ft. This depth is reduced to 0.15 ft for the fracture spacing of 50 feet, and reduced to only 0.07 ft for the small fracture spacing of 25 ft. This observation confirms the results from Fig. 23. For Case 1, water invasion is deeper, so the effect of formation damage is greater. The impact of fracturing-fluid induced formation damage may last several years.

Through this example, the accuracy of the hybrid approach that is based on the MINC method is demonstrated for both single-phase- and two-phase-flow problems. This approach can simulate the fracturing-fluid invasion into the tight matrix formation near the fracture faces in an SRV, and evaluate the impact of the formation damage caused by the fracturing-fluid invasion on the well performances. The connection between SRV and non-SRV zone is also considered for the simulation of fluid invasion during hydraulic fracturing and the backflow production. This approach is accurate compared to the very-fine meshed single-porosity simulation with explicit fracture discretization. Apart from the accuracy, the main advantage of this approach is the gain in CPU time. A simulation can be achieved within one minute (12 seconds in our case). So, this technique allows an operator to get a rapid response on the issue of formation damage related to hydraulic fracturing; it also to test sensitivity of various parameters on the well performance.

Finally, the proposed hybrid approach can easily be applied to a larger SRV case, because both the required number of gridblocks and the CPU time are small. We will consider, in future studies, the simulation of a very large SRV with, for example, 30 multistage fractures with the hybrid approach. This kind of problem is almost impossible to be simulated with an explicitly discretized fracture model. Also, future work will treat DFN. Note that the application of the MINC method is not limited to a regular network and also can be applied on an irregular one.

Discussion

To model a realistic reservoir fracture network, new type of model called a DFM has received great attention. This kind of model discretizes complex fracture networks explicitly. Many techniques with DFM models were tested and studied in the literature; most applicable models are called USDFM, EDFM, and iDFM (see, e.g., Lee et al. 2001; Karimi-Fard et al. 2006; Moinfar et al. 2011 and 2013; Norbeck et al. 2014).

		Single-Phase-Flow Simulations		Two-Phase-Flow Simulations			
Simulation Model	Case	No. of Grids	CPU Time	No. of Grids	CPU Time	Average Invasion Depth (ft)	Smaller Grid Volume (ft^3)
Explicit Discretized Fracture Model	Case 1	147,063	2 hours 12 minutes	147,063	5 hours 40 minutes	0.27	0.0003
	Case 2	396,579	8 hours	396,579	24 hours	0.15	
	Case 3	Not Simulated		Not Simulated			
Hybrid Approach	Case 1	1,039 (MINC6)	8.0 seconds	1,529 (MINC13)	12 seconds	0.27	120
	Case 2					0.15	240
	Case 3					0.07	480

Table 3—Comparison of CPU time between the explicit model and the hybrid approach for each case.

The ability of the hybrid approach with the MINC method was tested for the simulation of two-phase flow with a regular fracture network in this paper. Moreover, the MINC method is not limited to a regular fractured network, and can be extended to an irregular network (e.g., Pruess and Karasaki 1982). Future work will study multiphase-flow-modeling techniques with a DFN to simulate a realistic shale gas reservoir, where fracture-network complexity increases. The MINC method will be considered for better modeling concerning the matrix–fracture flow exchange in an irregular fracture network.

Conclusions

This paper discusses a hybrid approach that is based on the concept of the MINC method for simulation of gas production from unconventional shale gas reservoirs. This approach treats the interporosity flow entirely in a fully transient way for matrix–-fracture interaction. On the basis of the modeling results, the hybrid method provides very accurate simulations, compared with the finely meshed explicit discretized fracture model. An explicit discretized model is not suitable for unconventional reservoir simulations because of the computational intensity, especially for two-phase-flow problems. Using the hybrid approach that is based on the concept of the MINC method results in significant savings in the CPU time compared with an explicit discretized model.

The hybrid approach based on the MINC method can handle formation-damage issues in low-permeability reservoirs efficiently. The fracturing-fluid-induced formation damage, in particular, is studied. Simulation of fracturing-fluid invasion and its backflow need very-fine gridblocks near the fracture face for a better flow modeling into and from the fractures. This approach is suitable for the study of formation damage, as long as small block sizes are used near the fracture. The impact of formation damage may be great, depending on the depth of fracturing-fluid invasion into the matrix formation.

The hybrid approach is suitable for both single-phase- and multiphase-flow simulations in shale gas reservoirs. Moreover, it can be easily applied to a larger SRV case, which gives us the possibility to perform sensitivity tests (fracture apertures, fracture permeability, matrix permeability, and others) and to study advanced physical processes (adsorption and desorption, geomechanics aspect, Klinkenberg effect, and others), together with the formation-damage issue for field cases.

Nomenclature

a = matrix-block dimension
b = matrix-block dimension
k_{rg} = gas relative permeability
k_{rw} = water relative permeability
m_g = adsorption or desorption term per unit volume of formation
P = pressure
q = source/sink term
Q_p^{mf} = matrix–fracture interaction for phase p
S = fluid saturation
t = time
V_E = volume of adsorbed gas at standard condition per unit mass of solid
β = index of fluid phase
Φ = flow potential
v_β = volumetric velocity vector of fluid β
ϕ = effective porosity of formation
$\lambda_{p,ij}$ = mobility of phase p between gridblcoks i and j
μ = viscosity
σ = shape factor
ρ_r = solid-rock density
ρ_g = gas density

Subscripts

f = denote fracture
g = gas
m = denotes matrix
w = water

Acknowledgments

The authors gratefully acknowledge IFP Energies Nouvelles for their support. The first author would like to especially thank A. Khrouf for his contribution concerning the simulation part.

References

Agrawal, S. and Sharma, M. 2013. Liquid Loading Within Hydraulic Fractures and Its Impact on Unconventional Reservoir Productivity. Presented at the Unconventional Resources Technology Conference, Denver, 12–14 August. SPE 168781-MS. https://doi.org/10.2118/168781-MS.

Barenblatt, G. I., Zheltov, Iu. P., and Kochina, I. N. 1960. Basic Concepts in the Theory of Seepage of Homogeneous Liquids in Fissured Rocks. *Journal of Applied Mathematics and Mechanics* **24:** 1286–1303. https://doi.org/10.1016/0021-8928(60)90107-6.

Bertoncello, A., Wallace, J., Blytin, C. et al. 2014. Imbibition and Water Blockage in Unconventional Reservoirs: Well Management Implications During Flowback and Early Production, Vienna, Austria, 25–27 February. SPE-167698-MS. https://doi.org/10.2118/167698-MS.

Cheng, Y. 2012. Impact of Water Dynamics in Fractures on the Performance of Hydraulically Fractured Wells in Gas-Shale Reservoirs. *J Can Pet Technol* **51** (2): 143–151. SPE-127683-PA. https://doi.org/10.2118/127683-PA.

Cipolla, C. P., Lolon, E. P. Tathed, V. et al. 2009. Modeling Well Performance in Shale-gas Reservoirs. Presented at the SPE/EAGE Reservoir Characterization and Simulation Conference, Abu Dhabi, 19–21 October. SPE-125532-MS. https://doi.org/10.2118/125532-MS.

Clarkson, C. R. and Williams-Kovacs, J. D. 2012. Modelling Two-Phase Flowback of Multifractured Horizontal Wells Completed in Shale. Presented at the SPE Canadian Unconventional Resources Conference, Calgary, 30 October–1 November. SPE-162593-MS. https://doi.org/10.2118/162593-MS.

Delorme, M., Daniel, J. M., Kada-Kloucha, C. et al. 2013. An Efficient Model to Simulate Reservoir Stimulation and Induced Microseismic Events on 3D Discrete Fracture Network for Unconventional Reservoirs. Presented at the Unconventional Resources Technology Conference, Denver, 12–14 August. SPE 168726-MS. https://doi.org/10.2118/168726-MS.

Ding, D. Y., Langouet, H., and Jeanin, L. 2013. Simulation of Fracturing-Induced Formation Damage and Gas Production From Fractured Walls in Tight Gas Reservoirs. *Prod & Oper* **28** (3): 246–258. SPE-153255-PA. https://doi.org/10.2118/153255-PA.

Ding, D. Y., Wu, Y. S., Farah, N. et al. 2014. Numerical Simulation of Low-Permeability Unconventional Gas Reservoirs. Presented at the Unconventional Conference, Vienna, Austria, 25–27 February. SPE-167711-MS. https://doi.org/10.2118/167711-MS.

Ehrl, E. and Schueler, S. K. 2000. Simulation of a Tight-gas Reservoir With Horizontal Multifractured Wells. Presented at the SPE EUROPEC, Paris, 24–25 October. SPE-65108-MS. https://doi.org/10.2118/65108-MS.

Farhadinia, M. A. and Delshad, M. 2010. Modeling and Assessment of Wettability Alteration Processes in Fractured Carbonates Using Dual Porosity and Discrete Fracture Approaches. Presented at the SPE Improved Oil Recovery, Tulsa, 24–28 April. SPE-129749-MS. https://doi.org/10.2118/129749-MS.

Fazelipour, W. 2011. Development of Techniques to Integrate Hydraulic Fracturing Design and Reservoir Simulation Technologies—Application to Forecast Production of Stimulated Wells in Unconventional Gas Reservoirs. Presented at the Middle East Unconventional Gas Conference and Exhibition, Muscat, Oman, 31 January–2 February. SPE-142337-MS. https://doi.org/10.2118/142337-MS.

Friedel, T. 2004. *Numerical Simulation of Production From Tight-Gas Reservoirs by Advanced Stimulation Technologies*. PhD thesis, Freiberg University (July).

Gdanski, R., Fulton, D., and Chen, C. 2006. Fracture Face Skin Evolution During Cleanup. Presented at the SPE ATC&E, San Antonio, Texas, 24–27 September. SPE-101083-MS. https://doi.org/10.2118/101083-MS.

Geiger, S. T., Matthäi, S. K., Niessner, J. et al. 2009. Black-Oil Simulations for Three-Component, Three-Phase Flow in Fractured Porous Media. *SPE J.* **14** (2): 338–354. SPE-107485-PA. https://doi.org/10.2118/107485-PA.

Holditch, S. A. 1979. Factors Affecting Water Blocking and Gas Flow From Hydraulically Fractured Gas Wells. *J Pet Technol* **31** (12): 1515–1524. SPE-7561-PA. https://doi.org/10.2118/7561-PA.

Karimi-Fard, M., Gong, B., and Durlofsky, L. J. 2006. Generation of Coarse-Scale Continuum Flow Models From Detailed Fracture Characterizations. *Water Resources Research* **42** (10). https://doi.org/10.1029/2006WR005015.

Lee, S. H., Lough, M. F., and Jensen, C. L. 2001. Hierarchical Modelling of Flow in Naturally Fractured Formations With Multiple Length Scales. *Water Resources Research* **37** (3): 443–445. https://doi.org/10.1029/2000WR900340.

Li, J., Guo, B., Gao, D. et al. 2012. The Effect of Fracture-Face Matrix Damage on Productivity of Fractures With Infinite and Finite Conductivities in Shale-Gas Reservoirs. *SPE Drill & Compl* **27** (3): 348–354. SPE-143304-PA. https://doi.org/10.2118/143304-PA.

Lolon, E. P., Shaoul, J. R., and Mayerhofer, M. J. 2007. Application of 3D Reservoir Simulator for Hydraulically Fractured Wells. Presented at the Asia Pacific Oil and Gas Conference and Exhibition, Jakarta, 30 October–1 November. SPE-110093-MS. https://doi.org/10.2118/110093-MS.

Moinfar, A., Narr, W., Hui, M. H. et al. 2011. Comparison of Discrete-Fracture and Dual Permeability Models for Multiphase Flow in Naturally Fractured Reservoir. Presented at the Reservoir Simulation Symposium, The Woodlands, Texas, 21–23 February. SPE-142295-MS. https://doi.org/10.2118/142295-MS.

Moinfar, A., Varavei, A., Sepehnoori, K. et al. 2013. Development of a Coupled Dual Continuum and Discrete Fracture Model for the Simulation of Unconventional Reservoirs. Presented at the Reservoir Simulation Symposium, The Woodlands, Texas, 18–20 February. SPE-163647-MS. https://doi.org/10.2118/163647-MS.

Norbeck, J., Huang, H., Podgorney, R. et al. 2014. An Integrated Discrete Fracture Model for Description of Dynamic Behavior in Fractured Reservoirs. *Proc.,* 39th Workshop on Geothermal Reservoir Engineering, Department of Energy Resources Engineering, Stanford University, California, 24–26 February. SGP-TR-202.

Pruess, K. and Karasaki, K. 1982. Proximity Functions for Modeling Fluid and Heat Flow in Reservoirs With Stochastic Fracture Distributions. *Proc.,* 8th Workshop Geothermal Reservoir Engineering, Stanford University, Stanford, California, 14–16 December. SGP-TE-60

Pruess, K. and Narasimhan, T. N. 1983. A Practical Method for Modeling Fluid and Heat Flow in Fractured Porous Media. Presented at the Reservoir Simulation Symposium, New Orleans, 31 January–3 February. SPE-10509-MS. https://doi.org/10.2118/10509-MS.

Pruess, K. 1992. Brief Guide to the MINC-Method for Modeling Flow and Transport in Fractured Media. Technical report, Earth Sciences Division, Lawrence Berkeley Laboratory, University of California, May.

Rubin, B. 2010. Accurate Simulation of Non-Darcy Flow in Stimulated Fractured Shale Reservoirs. Paper presented at the SPE Western Regional Meeting held in Anaheim, California, USA, 27–29 May. SPE-132093-MS. https://doi.org/10.2118/132093-MS.

Sadrpanah, H., Charles, T., and Fulton, J. 2006. Explicit Simulation of Multiple Hydraulic Fractures in Horizontal Wells. Presented at the SPE Europec, Vienna, Austria, 12–15 June. SPE-99575-MS. https://doi.org/10.2118/99575-MS.

Schmid, K. S., Geiger-Boschung, S., and Sorbie, K. S. 2013. Higher Order FE-FV Method on Unstructured Grids for Transport and Two-Phase Flow With Variable Viscosity in Heterogeneous Porous Media. *Journal of Computational Physics* **241:** 416–444. https://doi.org/10.1016/j.jcp.2012.12.017.

Wang, J. Y., Holditch, S. A., and McVay, D. A. 2009. Modelling Fracture Fluid Cleanup in Tight-gas Wells. Presented at the Hydraulic Fracturing Technology Conference, The Woodlands, Texas, 19–21 January. SPE-119624-MS. https://doi.org/10.2118/119624-MS.

Warpinski, N. R., Mayerhofer, M. J., Vincent, M. C. et al. 2008. Stimulating Unconventional Reservoirs: Maximizing Network Growth While Optimizing Fracture Conductivity. Presented at the Unconventional Reservoirs Conference, Keystone, Colorado, 10–12 February. SPE-114173-MS. https://doi.org/10.2118/114173-MS.

Warren, J. E. and Root, P. J. 1963. The Behavior of Naturally Fractured Reservoirs. *SPE J* **3** (3): 245–255. SPE-426-PA. https://doi.org/10.2118/426-PA.

Wu, Y. S., Li, J., Ding, D. Y. et al. 2013. A Generalized Framework Model for Simulation of Gas Production in Unconventional Gas Reservoirs. Presented at the Reservoir Simulation Symposium, The Woodlands, 18–20 February. SPE-163609-MS. https://doi.org/10.2118/163609-MS.

Zidane, A. and Firoozabadi, A. 2014. An Efficient Numerical Model for Multicomponent Compressible Flow in Fractured Porous Media. *Advances in Water Resources* **74:** 127–147. https://doi.org/10.1016/j.advwatres.2014.08.010.

Appendix A: Numerical Scheme

A fully implicit discretization of Eqs. 2 and 3 on a cell i ($i=1,\ldots,N$) with a control-volume method is given by

$$\left[(\phi^m S^m_\beta \rho^m_\beta)_i^{(n+1)} + m_{(g,i)}^{(n+1)} - (\phi^m S^m_\beta \rho^m_\beta)_i^n - m^n_{(g,i)}\right]\frac{V_i}{\Delta t^{n+1}} - \sum_{i\in N_i}(F^m_{\beta,i,j})^{n+1} + (Q^{mf}_{\beta,i})^{n+1} - (Q^{mf}_{(\beta,i)})^{(n+1)} - (q^m_{(\beta,i)})^{(n+1)} \quad \text{(A-1)}$$

$$= \left[(\phi^f S^f_\beta \rho^f_\beta)_i^{n+1} - (\phi^f S^f_\beta \rho^f_\beta)_i^n\right]\frac{V_i}{\Delta t^{n+1}} - \sum_{j\in N_i}(F^f_{\beta,ij})^{n+1} - (Q^{mf}_{\beta,i})^{n+1} - (q^f_{\beta,i})^{n+1} = 0, \quad \text{(A-2)}$$

where $\beta = w$ or g; the superscript n denotes the previous time step and $n+1$ the current timestep to be solved; $\Delta t^{n+1} = t^{n+1} - t^n$; V_i is the volume of the cell i; N_i contains the set of direct neighboring cells j of cell i; $q_{\beta,i}$ is the sink/source term in cell i; Q_i^{mf} is the flow exchange between matrix and fracture media in cell i; and $F_{\beta,i,j}$ is the flow term between cells i and j, calculated with a two points flux-approximation scheme,

$$(F^\alpha_{\beta,ij})^{n+1} = (\lambda^\alpha_{\beta,ij})^{n+1} T_{ij}[\Phi^{\alpha,n+1}_{\beta,j} - \Phi^{\alpha,n+1}_{\beta,i}], \quad \text{(A-3)}$$

where $\alpha = m$ or f, T_{ij} is the transmissibility between cells i and j; $\lambda^\alpha_\beta = \dfrac{\rho_\beta(P^\alpha_\beta) kr^\alpha_\beta(S^\alpha_\beta)}{\mu_\beta(P^\alpha_\beta)}$ is the mobility term of phase β, calculated with an upstream scheme; k is the absolute permeability; and Φ is the potential, given by

$$\Phi^{\alpha,n+1}_{\beta,i} = P^{\alpha,n+1}_{\beta,i} + \rho_\beta(P^{\alpha,n+1}_{\beta,i}) g z_i, \quad \text{(A-4)}$$

with g the gravitational acceleration and z the vertical coordinate. For a DP and single-permeability approach, $F^m_{\beta,ij} = 0$.

The flow-exchange term Q_i^{mf} is calculated with

$$(Q^{mf}_{\beta,i})^{n+1} = \sigma(\lambda^{mf}_{\beta,i})^{n+1}(\Phi^{m,n+1}_{\beta,i} - \Phi^{f,n+1}_{\beta,i}), \quad \text{(A-5)}$$

with σ being the shape factor.

The system of Eqs. 2 and 3 contains four equations (with $\beta = w$ and g), and eight unknowns, P^m_g, P^m_w, P^f_g, P^f_w, S^m_g, S^m_w, S^f_g, and S^f_w. To complete this system, we use capillary pressures,

$$P^m_c(S^m_g) = P^m_g - P^m_w \quad \text{(A-6)}$$

$$P^f_c(S^f_g) = P^f_g - P^f_w \quad \text{(A-7)}$$

and saturation relations,

$$S^m_w + S^m_g = 1 \quad \text{(A-8)}$$

$$S^f_w + S^f_g = 1. \quad \text{(A-9)}$$

In practice, we consider that the gas pressures P_g^m, P_g^f and the water saturations S_w^m, P_w^f are main variables, and the water pressures and the gas saturations are secondary variables computed with Eqs. A-6 through A-9.

In a fully implicit scheme, all parameters in the system of Eqs. A-1 and A-2 are functions of pressures and saturations at time $n+1$ with $\varphi^\alpha = \varphi^\alpha(P_g^{\alpha,n+1})$, $\rho_\beta^\alpha = \rho_\beta(P_\beta^{\alpha,n+1})$, $m_g = m_g(P_g^{m,n+1})$, $kr_\beta^\alpha = kr_\beta^\alpha(S_w^{\alpha,n+1})$, $\mu_\beta = \mu_\beta(P_\beta^{\alpha,n+1})$, ...

Using the relations of Eqs. A-6 through A-9, the left-hand side of system of Eqs. A-1 and A-2 can be written in a general form as a function of $P_g^{m,n+1}$, $P_g^{f,n+1}$, $S_w^{m,n+1}$ and $S_w^{f,n+1}$,

$$R_{\beta,i}^{\alpha,n+1} = R_{\beta,i}^{\alpha,n+1}(\vec{X}) \quad \ldots\ldots\ldots\ldots \quad \text{(A-10)}$$

for $\beta = w$ and g; $\alpha = m$ and f; $i = 1, \ldots, N$ with N the number of grid cells, where $\vec{X} = (P_{g,1}^{m,n+1}, P_{g,1}^{f,n+1}, S_{w,1}^{m,n+1} S_{w,1}^{f,n+1}, \ldots, P_{g,N}^{m,n+1}, P_{g,N}^{f,n+1}, S_{w,N}^{m,n+1}, S_{w,N}^{f,n+1})$.

We want to find $\vec{X}$ so that

$$R_{\beta,i}^{\alpha,n+1}(\vec{X}) = 0 \quad \ldots\ldots\ldots\ldots \quad \text{(A-11)}$$

This is a nonlinear system. Note that we have $4 \times N$ equations and $4 \times N$ unknowns. To solve this system, we use the Newton-Raphson method. The Newton iteration scheme gives rise to

$$\sum_m \frac{\partial R_{\beta,i}^{\alpha,n+1}(\vec{X}_p)}{\partial x_m}(x_{m,p+1} - x_{m,p}) = -R_{\beta,i}^{\alpha,n+1}(\vec{X}_p), \quad \ldots\ldots\ldots\ldots \quad \text{(A-12)}$$

where x_m is the m^{th} component of the vector $\vec{X}$ ($m = 1, \ldots, 4N$) and p is the Newton iteration level. This is a linearized equation with $\vec{X}_0 = (P_{g,1}^{m,n}, P_{g,1}^{f,n}, S_{w,1}^{m,n}, S_{w,1}^{f,n}, \ldots, P_{g,N}^{m,n}, P_{g,N}^{f,n}, S_{w,N}^{m,n}, S_{w,N}^{f,n})$ (when $p = 0$, we use the values at the previous timestep). In this system, $\vec{X}_p$ is known, and $\vec{X}_{p+1}$ is the unknown to be solved. The key issue of the Newton-Raphson method is the computation of the derivative $\frac{\partial R_{\beta,i}^{\alpha,n+1}(\vec{X}_p)}{\partial x_m}$ to construct the Jacobian matrix. At each Newton iteration, Eq. A-12 represents a system of $4 \times N$ linearized equations with a sparse matrix, which is solved by a linear solver. Letting M be the Jacobian matrix, Eq. A-12 becomes

$$M(\vec{X}_{p+1} - \vec{X}_p) = -R_{\beta,i}^{\alpha,n+1}(\vec{X}_p), \quad \ldots\ldots\ldots\ldots \quad \text{(A-13)}$$

so

$$\vec{X}_{p+1} = \vec{X}_p - M^{-1} R_{\beta,i}^{\alpha,n+1}(\vec{X}_p). \quad \ldots\ldots\ldots\ldots \quad \text{(A-14)}$$

The Newton iteration process continues until the residuals $R_{\beta,i}^{\alpha,n+1}$ or changes in the primary variables $\vec{X}_{p+1} - \vec{X}_p$ over iteration are reduced below preset convergence tolerances.

Nicolas Farah is a PhD degree student at IFP Energies Nouvelles based in Rueil-Malmaison, France. His research interests include reservoir simulation and characterization, numerical modeling, and unconventional hydrocarbon reservoirs. Farah holds a BS degree in physics from Lebanese University (Lebanon) and a Diploma of Engineering in Mechanics and Energetics from École Polytechniques de Marseille (France) and an MS degree in petroleum engineering from UPPA University (France).

Didier Yu Ding is a senior research engineer at IFP Energies Nouvelles in Rueil-Malmaison, France. His research interests include reservoir simulation and characterization, numerical modeling, and unconventional hydrocarbon reservoirs. Ding holds a BS degree in mathematics from Peking University (China) and MS and PhD degrees in applied mathematics from the University of Paris (France).

Yu-Shu Wu is a professor and Foundation CMG Reservoir Modeling Chair and the director of Energy Modeling Group (EMG) research center in the Petroleum Engineering Department at the Colorado School of Mines (CSM). He is a fellow of the Geological Society of America. At CSM, Wu teaches and carries out research in reservoir engineering, multiphase fluid and heat flow, geomechanics, unconventional oil and gas reservoir dynamics, CO_2 geosequestration and EOR, geothermal engineering, and numerical reservoir simulation. He leads the EMG in its research effort in (1) flow dynamics in unconventional oil and gas reservoirs; (2) coupled processes of multiphase fluid and heat flow, geomechanics, and chemical transport in porous and fractured media; (3) CO_2 sequestration and EOR application; (4) improved formation stimulation/cryogenic fracturing technologies; and (5) advanced reservoir-simulation technologies. Previously, Wu was a staff scientist with the Earth Sciences Division of Lawrence Berkeley National Laboratory for 14 years (1995–2008). During his career, he has authored or coauthored 100 + peer-reviewed journal papers and 17 peer-reviewed books/chapters as well as 55 SPE papers.